Loss Prediction in DC-Biased Magnetic Sheets

Loss prediction in DC-biased magnetic sheets.

O. de la Barrière[1], C. Ragusa[2], C. Appino[3], F. Fiorillo[3]

[1]SATIE, ENS Cachan, CNRS, UniverSud, 61 av. du Président Wilson, F-94230 Cachan, France
[2]Department of Energy, Politecnico di Torino, C.so Duca degli Abruzzi 24, 10129 Torino, Italy
[3]Istituto Nazionale di Ricerca Metrologica (INRIM), Strada delle Cacce 91, 10135 Torino, Italy

Power losses in soft magnetic materials can be solidly assessed by the Statistical Theory of Losses (STL), which provides physical foundation to the concept of loss separation. The theory is however limited to the conventional case of symmetric hysteresis loops and cannot be straightforwardly applied for a magnetic core operating under a DC bias. We show in this paper that such constraint can be released by combining the STL with a simplified approach to the Dynamic Preisach Model. This approach leads to the more affordable Static Preisach Model, with largely reduced computation time. In this way the hysteresis and excess loss components, with and without DC bias, are identified and calculated starting from a minimum set of experimental data. We provide a wide-ranging experimental validation of the theory, which is applied to the behavior of the energy loss versus frequency, measured up to f = 1 kHz, in non-oriented and grain-oriented iron-silicon sheets and in iron-cobalt alloys, subject to different polarization bias levels.

***Index Terms*—Magnetic losses, magnetic steel sheets, Preisach model, DC-biased induction.**

1. Introduction

The electromagnetic models of electrical machines and their optimization pass through modeling of iron losses and the related numerical implementation, a complex task, where the physical problem compounds with the efficiency of the computational approach. Different loss models are today available, by which a different compromise between computation complexity and predicting accuracy is attained. Such models, however, are typically developed for the standard case of sinusoidal induction and symmetric magnetization cycles. But a variety of excitation regimes take place in actual cores. Non-sinusoidal induction waveforms ubiquitously arise or are imposed (e.g. Pulse Width Modulation) in inductors and electrical machines, two-dimensional flux loci are always created in motors and generators, and DC-biased magnetization regimes occur in a relevant number of applications. The latter working condition is typical of inductive components used in power electronics (e.g., switch-mode power supplies [1], [2], dc-dc buck converters [3], [4], pulse transformers, etc.), power transformers in high-voltage DC transmission lines [5], stator and rotor of permanent magnet machines [6], [7], stator core of switched reluctance motors (SRM) [8], [9]. Fig. 1 provides a cross-sectional view of a three-phase SRM. The electronically driven energizing currents have here unipolar character and the radial induction in the salient stator poles has a strong DC bias, because the induction waveform evolves from zero to its positive maximum value. The whole stator of this machine is actually excited by similar DC bias waveforms. The case of the Pulse Width Modulation (PWM) [10], [11] can also be seen as a problem of polarized induction waveform, being possible to equate the minor loops associated to PWM with DC-biased cycles. The example in Fig. 2 shows how an imposed polarization bias J_b = 0.75 T modifies shape and area of a quasi-static symmetric hysteresis loop of peak amplitude $J_p = \pm 0.50$ T taken in a non-oriented Fe-Si sheet. The physical reason for the observed large increase of the loop area (i.e. the loss) brought about by the bias is understood by looking at the mechanism of the magnetization process. The $J(H)$ behavior can in fact be regarded as the macroscopic outcome of a sequence of microscopic magnetic transitions between metastable states, the Barkhausen jumps, and their statistical properties. Such properties can be lumped into a distribution function $p(\delta F, \delta E)$ for the free energy variation δF and the dissipated energy δE characterizing the jumps [12]. The existence of a distribution $p(\delta F, \delta E)$ implies that a distribution $p(h_u, h_c)$ exists for the effective local field h_u and the extra field h_c triggering the transition (local coercive field). The higher the peak polarization level J_p attained during symmetric cycling, the wider is the covered $p(h_u, h_c)$ region and the higher is the measured macroscopic coercive field H_c. This implies, as actually observed, that the hysteresis loss W_{hyst} will increase more than linearly with J_p. The power law $W_{hyst} \propto J_p^m$, with $m > 1.5$ is generally found, which justifies the shown increase of W_{hyst} when the hysteresis loop is made to drift towards higher h_u values by DC biasing.

The scenery of the magnetization process as a train of Barkhausen discontinuities finds a natural mathematical counterpart in the Preisach model of hysteresis and the related statistics of the irreversible transitions. These are represented as elementary rectangular hysteresis loops (hysterons)

Manuscript received March 15, 2019; revised March 15, 2019 and March 15, 2019, accepted March 15, 2019. Date of publication March 15, 2019; date of current version March 15, 2019. Corresponding author: C. Appino (e-mail: c.appino@inrim.it).

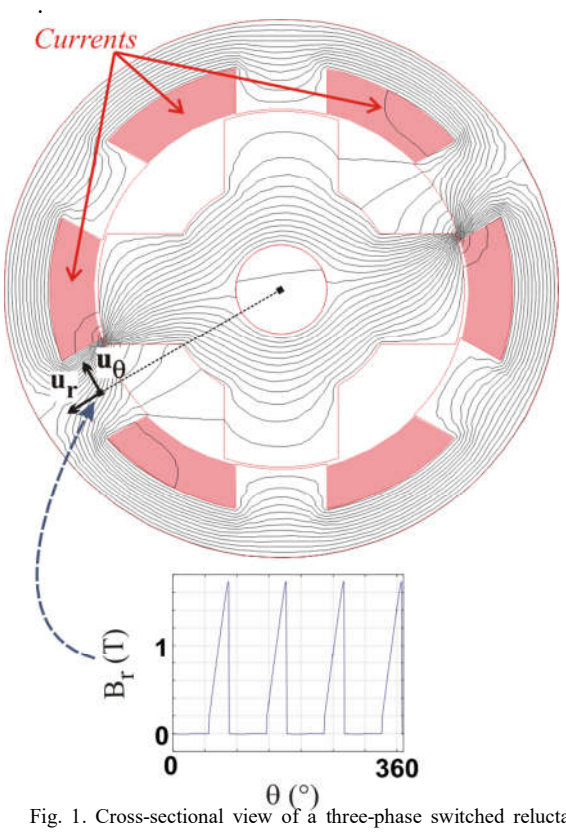

Fig. 1. Cross-sectional view of a three-phase switched reluctance motor. The radial component B_r of the induction in the salient stator poles has unipolar character and is associated with an asymmetric hysteresis loop.

switching between the saturated states $\pm J_s$ when the changing effective field passes through the values $h_u \pm h_c$. In the customary approach to hysteresis loop prediction, which provides for easy graphical representation, the fields $\alpha = h_u + h_c$ and $\beta = h_u - h_c$ are introduced. The asymmetric hysteresis loop is then calculated by determining the distribution function $p(\alpha,\beta)$ and integrating it over the appropriate region in the (α,β) plane. Finding the Preisach Distribution Function (PDF) $p(\alpha,\beta)$ (identification problem) is the key step in modeling [12], [13]. The factorization property

$$J_s\, p_{irr}(\alpha,\beta) = \varphi(\alpha)\varphi(-\beta) \qquad (1)$$

is generally assumed in steels sheets for the distribution of the hysteron switching fields. The whole PDF, taking into account also the reversible processes is expressed as $p(\alpha, \beta)= p_{irr}(\alpha, \beta) + p_{rev}(\alpha)\delta(\alpha-\beta)$, with $\delta(\alpha-\beta)$ the Dirac delta function. Typically, the PDF is reconstructed by measuring either a number of centered minor loops or first-order recoil curves [13], but appropriate analytic functions are often shown to apply [12]. The dashed lines in Fig. 2 provide an example of symmetric and asymmetric quasi-static hysteresis loop fitting in NO steel sheets using a so found PDF. It is stressed that the biased loop is the outcome a well-defined history in the (J, H) domain, and is calculated following a defined trajectory in the (α,β) Preisach plane. But by this procedure we cover only part of the problem, because we are interested in the overall response, static and dynamic, of the material. We wish, in particular, to predict the energy loss dependence on frequency and the way it is modified by a DC bias. In doing so, we will make reference to a defined physical framework, the one jointly offered by the Static Preisach Modeling (SPM) and the Statistical Theory of Losses [12].

Efforts have been devoted in the literature to the assessment of the magnetic losses in soft magnetic materials subjected to DC bias. Most investigations are based on the use

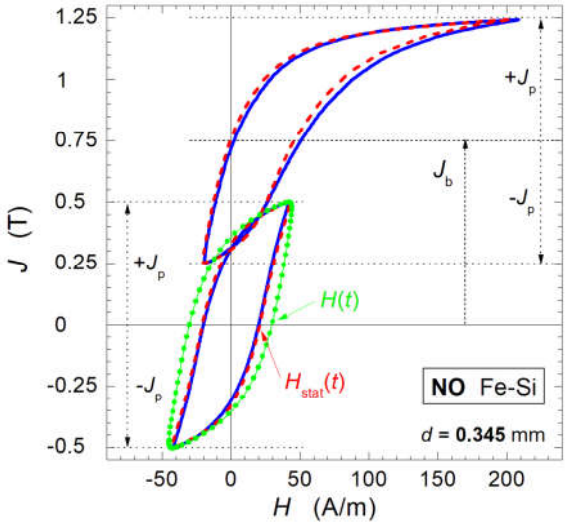

Fig. 2. The unbiased quasi-static hysteresis loop (f = 2 Hz) of amplitude J_p = ± 0.50 T, measured in a non-oriented Fe-(3.5 wt%)Si sheet, modifies into asymmetric and wider loop upon DC biasing (J_b = 0.75 T). This evolution is predicted by Preisach modeling (dashed lines). The outer symmetric loop (green curve) with J_p = ± 0.50 T is measured at f = 100 Hz.

of the Steinmetz equation, generally assumed as a simple analytical expression for the power loss versus frequency and peak induction B_p

$$P(B_p, f) = k\, f^a B_p^b, \qquad (2)$$

where k, a, and b are material dependent parameters. It is a fully empirical formulation, commonly used in problems of electrical engineering under conventional supply conditions [14]. As such, it lacks flexibility and suitable modifications of (2) and/or dependence of k, a, and b on the measuring parameters (particularly DC-field H_{DC} and B_p) are generally introduced [4], [14]-[18]. Consequently, a large number of pre-emptive measurements in the presence of H_{DC} are required, leading more to an *ad hoc* description of specific behaviours of the material than to a predictive formulation. The Steinmetz's approach may also call for further experiments and additional fitting parameters when non-sinusoidal induction (e.g., triangular, trapezoidal) is treated [19], [20].

Loss separation [21] has also been invoked for modelling the effect of DC bias, either disregarding the excess loss component and fitting the results by a number of arbitrary constants [22], [23] or by lumping it in the Jiles-Atherton model of magnetic hysteresis [24]. Again, the fitting parameters are empirically expressed and adjusted in order to provide the best representation of the measured asymmetric

loops. The specific hysteretic history in the (J, H) plane leading to the minor loop with polarization swing $\pm J_p$ under biasing by the DC field H_{bias} is generally ignored. We actually know that the base formulation of the Preisach model, with a stable, material dependent only, distribution $p(\alpha,\beta)$, predicts congruence of the minor loops, that is, a unique solution for any (H_{bias}, $\pm J_p$) [13]. The experiments show, however, that this is only approximately true, a fact related to the evolving role of the internal magnetostatic fields. Refined results are consequently obtained by adopting a moving distribution $p(\alpha + kJ, \beta + kJ)$, with k a constant and kJ the "moving field" [25].

The Preisach model, far from being a mere mathematical tool, can be associated with real processes at the scale of domain walls (dws) and their motion across a stochastic energy landscape [26]. It occurs then that under dynamic conditions the elementary dw transitions, subjected to a rate-dependent frictional (e.g. eddy-current related) counterfield, take place in a finite time interval and its mathematical embodiment, the hysteron, is accordingly modified [27]. This is the starting idea of the Dynamic Preisach Model (DPM), the physically based dynamic extension of the Static Preisach Model (SPM) developed by Bertotti [28]. The DPM has a broad domain of application and permits one to predict energy loss and hysteresis loop in steel sheets under sinusoidal and non-sinusoidal induction. It can also be adapted to the loss calculation in the presence of skin effect [29]. However, it requires heavy numerical implementation, because one must compute at each instant of time the state of each switching Preisach hysteron. An example of DPM application by use of Finite Element Method (FEM) analysis in DC-biased nonoriented Fe-Si sheets up to a few kHz is discussed in [30]. The case of PWM waveforms with $2n$ minor loops of peak-to-peak amplitude $2J_p$ nested into a major loop was treated in [31] by combination of the SPM and the Statistical Theory of Losses (STL). The hysteresis loss component W_{hyst}, the sum of the areas of the major loop and the $2n$ biased minor loops, is in this case calculated by the SPM. The classical energy loss $W_{class}(f)$ is at the same time expressed, by assuming uniform reversal of the magnetization across the sheet cross-section at the macroscopic scale, by the equation

$$W_{\mathrm{class}}(f) = \sigma \frac{d^2}{12} \int_0^{1/f} \left(\frac{\mathrm{d}J}{\mathrm{d}t}\right)^2 \mathrm{d}t\,, \qquad (3)$$

where σ is the material conductivity and d is the sheet thickness. It is noted that $W_{class}(f)$ is expressed in (3) in terms of J, because we assume here that, to any practical extent, polarization and induction coincide. According to (3), $W_{class}(f)$ *is independent of the DC bias.* But this is not the case for the whole dynamic loss $W_{dyn}(f) = W(f) - W_{hyst}$, which is always observed to increase with H_{bias}. This finding is then justified in terms of increase of the excess loss $W_{exc}(f) = W_{dyn}(f) - W_{class}(f)$. We write, according to the STL,

$$W_{\mathrm{exc}}(f) = \sqrt{\sigma G S V_0(J_p, J_b)} \int_0^{1/f} \left|\frac{\mathrm{d}J}{\mathrm{d}t}\right|^{3/2} \mathrm{d}t, \qquad (4)$$

where $G = 0.1356$, S is the cross-sectional area of the sheet sample, and the statistical parameter $V_0(J_p, J_b)$, related to the distribution of the local coercive fields [21], is a function of both peak J_p and bias J_b polarization values.

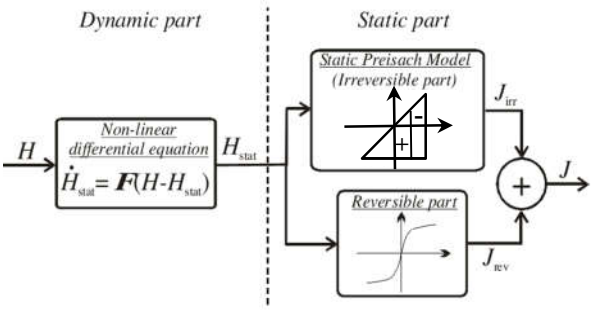

Fig. 3. The operator $\boldsymbol{F}$ permits one to retrieve the quasi-static field H_{stat} providing, under quasi-static excitation, the same irreversible polarization level J_{irr} achieved at a generic working frequency f under the dynamic field H, as defined in (5). By adding the reversible contribution J_{rev}, the dynamic polarization $J(f)$ is calculated using the Static Preisach Model (SPM) of hysteresis.

We will show in the following that the problem of dealing with the dynamic losses under bias can be treated and analytically formulated by bringing the description of the dynamic magnetization back to the SPM, thereby reducing to dramatic extent the computational burden required by the DPM. In particular, a connection is worked out between the SPM and the statistical parameter $V_0(J_p,J_b)$, whose dependence on the DC bias is eventually obtained, together with that of W_{exc}. Little pre-emptive material data are required, namely the quasi-static return magnetization curve from technical saturation for implementing the SPM and a couple of power loss values at two different frequencies under unbiased sinusoidal flux for the STL. The theory, applied to a number of measurements performed with and without H_{bias} up to 1 kHz on non-oriented Fe-Si and Fe-Co and grain-oriented Fe-Si sheets, shows good predicting ability.

2. The theoretical model

The physical scheme of the magnetization process as a sequence of local magnetization reversals associated with a distribution of switching fields is shared by the Preisach model and the STL. One can assimilate, in particular, the Preisach hysterons with the Magnetic Objects of the STL and the dynamics of their reversal behavior, where the time dependent applied field is balanced by the local threshold field and the eddy current field. For any macroscopic magnetization value, a correlation exists between static and dynamic fields, a property we shall make explicit in the following by formulating a solution for the prediction of the loss under bias in terms of quasi-static hysteresis loop and SPM. The overall scheme of this approach is sketched in Fig. 3. Starting from the DPM and making appropriate simplifications, a differential equation describing the dynamic effects of the material is worked out, permitting one to calculate W_{exc} in the presence of a DC bias. Since a semi-analytical expression for the quasi-static loss W_{hyst} can be derived and W_{class} is known from (3), the total loss $W(f) = W_{hyst} + W_{class}(f) + W_{exc}(f)$ is obtained.

2.1 Dynamic versus Static Preisach Model.

A simplified dynamic hysteresis model, neglecting the moving field, is here derived, limited to the frequency domain where the skin effect is irrelevant. It is partly based on previous calculations developed in [32], [33]. We start by defining the effective dynamic field

$$H(t) = H_a(t) - H_{dem}(t) - H_{class}(t), \qquad (5)$$

the difference between the applied field H_a, the demagnetizing field H_{dem}, and the counterfield H_{class} (classical field) generated by the macroscopic eddy currents. The latter is proportional to the measured induction derivative, according to

$$H_{class}(t) = \sigma \frac{d^2}{12} \cdot \frac{dJ}{dt}. \qquad (6)$$

Let us then consider the magnetization process by hysteron transitions in the Preisach plane, as sketched in Fig. 4. The coordinates α and β in this plane are the threshold (coercive) local fields, including the interaction fields, for the hysteron transition under ascending and descending applied field, respectively. For any (α, β) we calculate, at each instant of time, the state function Ψ, which is defined according to the following equation

$$\frac{d\Psi(\alpha,\beta;t)}{dt} = \begin{cases} k_d(H(t) - \alpha) & \text{if } H \geq \alpha \\ k_d(H(t) - \beta) & \text{if } H \leq \beta \\ 0 & \text{if } \beta < H < \alpha \end{cases}, \qquad (7)$$

where k_d is the so-called DPM constant [28] and the normalized flux Ψ varies between [-1; +1]. Equation (7) brings forth the fact that the hysteron transition occurs at a finite rate of change, proportional to the difference between the dynamic field $H(t)$ and the threshold field. With dH/dt = const., $\Psi(t)$ increases with time according to a quadratic law $\Psi(\alpha; t) \propto (H(t) - \alpha)^2$ within the transition region (H - ΔH, H), the faster $H(t)$ the wider ΔH. This region shrinks into a line under quasi-static magnetization, the total polarization value $J(t)$ remaining unchanged, because the transition occurs in a step-like fashion at the effective static field H_{stat}. *By making explicit the relationship between H(t) and H_{stat}(t), the SPM becomes available for calculating dynamic loops and losses*. The total polarization $J(t)$, the sum of the irreversible $J_{irr}(t)$ and reversible $J_{rev}(t)$ contributions, can be expressed, under very general terms as [13]

$$J(H(t)) = J_s \iint_{\alpha \geq \beta} p(\alpha,\beta)\, \Psi(\alpha,\beta;H(t))\, d\alpha\, d\beta \quad . \qquad (8)$$

If we refer to the ascending major branch of the loop taken between $-\alpha_{lim}$ and $H(t)$ in Fig. 4, we can then write, introducing the reversible permeability $\mu_{rev}(H) = dJ_{rev}/dH$,

$$J(H(t)) = J_{irr}(t) + J_{rev}(t) =$$
$$= J_s \int_{-\alpha_{lim}}^{\alpha_{lim}} d\alpha \int_{-\beta_{lim}}^{\alpha} \Psi(\alpha,\beta;t) p_{irr}(\alpha,\beta) d\beta +$$
$$+ \left(\int_{-\alpha_{lim}}^{H(t)} \mu_{rev}(\alpha) d\alpha - \Delta J_{rev}\right), \qquad (9)$$

where ΔJ_{rev} is the reversible contribution to J at saturation. We note here that the experimental knowledge of the reversible permeability $\mu_{rev}(H)$ provides a shortcut to the use of the distribution function $p_{rev}(\alpha)\delta(\alpha-\beta)$ in the calculation of $J_{rev}(t)$ in (9). Implementation of (8) requires a burdensome computational process, in contrast with the manageable calculations required by the SPM and its solidly assessed applications, which take advantage of the Everett function formalism [13]. As previously stressed and sketched in Fig. 4, the dynamic field value $H(t)$ is related to the value of the static field $H_{stat}(t)$. By connecting these two fields, we will be able to calculate $J(t)$ under dynamic conditions using the SPM, according to the scheme shown in Fig. 3.

2.2 The relationship between H(t) and H_{stat}(t)

The hysteron transition strip of width ΔH in the Preisach plane (α, β) lies along either the α or the β axis, according to whether $H(t)$ is decreasing or increasing. In the latter case, shown in Fig. 4, the transition strip moves towards $H = \alpha_{lim}$, leaving on its trail the fully reversed (+) hysterons. We wish to quantitatively describe this process, to find, in particular, the differential operator ***F*** connecting the dynamic and static fields $H(t)$ and $H_{stat}(t)$. This objective is achieved through the procedure described in Appendix A, where simple analytical formulations are worked out. The starting point consists in equating the static and dynamic polarization values attained with $H_{stat}(t)$ and $H(t)$, respectively, through the corresponding integrals in the Preisach plane. With some simplifications (i.e., by assuming dH/dt and the differential permeability uniform across the transition strip), we obtain that the width ΔH

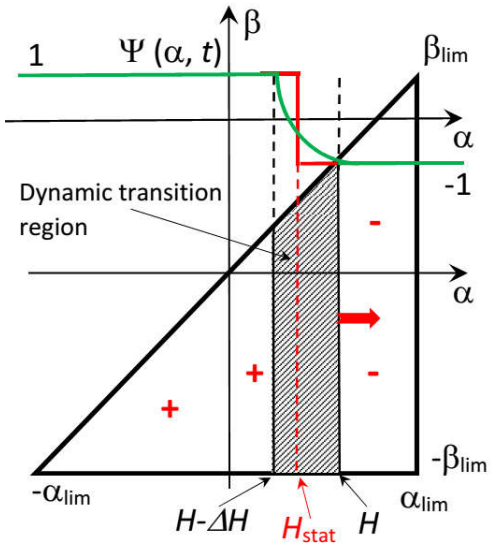

Fig. 4. Dynamic evolution of the magnetization process under a time increasing effective field $H(t)$ and its representation in the Preisach plane. The transition region of width ΔH identifies the ensemble of hysterons smoothly switching at a given instant of time t between the normalized flux states Ψ = [-1, +1]. The width ΔH of the dynamic transition strip increases with increasing the field rate of change dH/dt, according to $\Delta H = sign(dH_{stat}/dt) \cdot 2\sqrt{\frac{1}{k_d}\left|\frac{dH_{stat}}{dt}\right|}$, with k_d a constant. It shrinks into a line of coordinate $\alpha = H_{stat}$ under quasi-static excitation, with the parabolic behavior of the flux $\Psi(\alpha)$ changing into a step-like transition.

increases with the rate of change dH/dt, that is with dH_{stat}/dt, according to

$$\Delta H = sign(\mathrm{d}H_{\mathrm{stat}}/\mathrm{d}t)\cdot 2\sqrt{\frac{1}{k_{\mathrm{d}}}\left|\frac{\mathrm{d}H_{\mathrm{stat}}}{\mathrm{d}t}\right|} \qquad (10)$$

and that $H_{stat}(t)$ takes the value

$$H_{\mathrm{stat}}(t) = H(t) - (2/3)\Delta H. \qquad (11)$$

It is then concluded that $H_{stat}(t)$ and $H(t)$ are related by the differential equation

$$\mathrm{d}H_{\mathrm{stat}}/\mathrm{d}t = sign[H(t) - H_{\mathrm{stat}}(t)]\frac{9}{16}k_{\mathrm{d}}[H(t) - H_{\mathrm{stat}}(t)]^2 \qquad (12)$$

where *sign* = +1 (-1) for $\mathrm{d}H_{\mathrm{stat}}/\mathrm{d}t > 0$ ($\mathrm{d}H_{\mathrm{stat}}/\mathrm{d}t < 0$). For the ascending branch of the cycle, we obtain

$$H(t) = H_{\mathrm{stat}}(t) + \frac{4}{3}\sqrt{\frac{1}{k_{\mathrm{d}}}\left|\frac{\mathrm{d}H_{\mathrm{stat}}}{\mathrm{d}t}\right|}, \qquad (13)$$

where the second term on the right hand side represents the excess field H_{exc}. We recognize here the role of the DC bias on the excess loss through its effect on $\mathrm{d}H_{\mathrm{stat}}/\mathrm{d}t$. The bias brings in fact the system towards higher switching fields, that is, larger swing of H_{stat} across the loop for any given J_p value. $\mathrm{d}H_{\mathrm{stat}}/\mathrm{d}t$ is correspondingly increased and, according to (13), the same is for H_{exc} and, consequently, for the dynamic loss $W_{dyn}(f) = W(f) - W_{hyst}$.

This conclusion is at odds with the general notion of energy loss depending on the DC bias only through the change of the quasi-static component [17], [22], [23]. Such assumption amounts to state that, with defined flux waveform and J_p value, the dynamic loss solely depends on the induction (polarization) derivative. There is experimental evidence that this is not the case [4] [33]. The physically based STL has the property of bringing to light the connection between the static and dynamic magnetization processes, that is, the fields $H(t)$ and $H_{stat}(t)$. This result is unattainable by purely empirical or phenomenological models.

In the phenomenological Dynamic Hysteresis Model of S.E. Zirka, et al. [34], [35], the instantaneous value of the applied field $H(t)$ in thin soft steel sheets is postulated to obey either the equation

$$H(t) = H_{\mathrm{stat}}(B) + K_{\mathrm{clas}}\frac{\mathrm{d}B}{\mathrm{d}t} + g_{\mathrm{exc}}(B)\left(\frac{dB}{dt}\right)^{\alpha_{\mathrm{exc}}(B_{\mathrm{p}})} \qquad (14)$$

or the equation

$$H(t) = H_{\mathrm{stat}}(B) + g_{\mathrm{dyn}}(B)\left(\frac{dB}{dt}\right)^{\alpha_{\mathrm{dyn}}(B_{\mathrm{p}})} \qquad (15)$$

(ascending branch), where $K_{clas} = \sigma d^2/12$ and $g_{exc}(B)$, $\alpha_{exc}(B_p)$, $g_{dyn}(B)$, and $\alpha_{dyn}(B_p)$ are suitable fitting functions. They are identified, for any B_p value, by resorting to a best fitting procedure of few hysteresis loops measured at different frequencies. In this way, minor asymmetric loops, as imposed by induction waveforms with local minima (e.g. two-level PWM votage), are described, though the dependence on the polarization bias is not explicitly provided.

2.3 *The DC-bias and the Statistical Theory of Losses.*

The identification of the hysteron transition with the reversal dynamics of the Magnetic Objects (MOs), which can be written, in terms of normalized flux derivative, as [27]

$$\frac{\mathrm{d}\Psi}{\mathrm{d}t}(\alpha;t) = k_{\mathrm{d}}(H(t)-\alpha) = \frac{N_0}{\sigma G S J_{\mathrm{s}}}(H(t) - \alpha) \qquad (16)$$

where N_0 is the total number of MOs contained in the cross-sectional area of the sheet sample, permits us to quantitatively connect the results of the STL with the DPM, by posing $k_{\mathrm{d}} = N_0/\sigma G S J_{\mathrm{s}}$ in (7). For a polycrystalline material of average grain size $\langle s\rangle$ we can pose $\langle s\rangle \sim S/N_0$ and

$$k_{\mathrm{d}} \sim \frac{1}{\sigma G \langle s\rangle J_{\mathrm{s}}}. \qquad (17)$$

The STL is easily implemented, because it requires minimum pre-emptive measurements under sinusoidal induction, while permitting one to treat the magnetic losses under distorted and generally non-sinusoidal induction [31], [36], [37], very high inductions [38], high frequencies [39], [40] and two-dimensional flux [41], [42]. In the absence of bias, the procedure, as described in detail in [31], is based on the measurement, for any given J_p and sinusoidal induction, of $W(J_p, f)$ at two frequencies. This permits one to determine, once $W_{class}(J_p, f)$ is calculated, $W_{hyst}(J_p)$ and the parameter $V_0(J_p)$, that is $W_{exc}(J_p, f)$, and accomplish the loss separation upon the whole frequency range.

Wishing to extend this approach to the loss decomposition of $W(J_p, f)$ over a range of bias values J_b, we would need to repeat the previous procedure, that is, to determine the quantities $W_{hyst}(J_p, J_b)$ and $V_0(J_p, J_b)$ upon the whole desired set of J_b values. This lengthy approach can be circumvented by resorting, thanks to the previously discussed relationship between static and dynamic magnetization parameters, to the SPM. In the following we will show, in particular, that the energy loss versus frequency under bias $W(J_p, J_b, f)$ can be predicted using, at the cost of reasonable approximations, analytical formulations for $W_{hyst}(J_p, J_b)$ and $V_0(J_p, J_b)$.

2.4 The hysteresis loss $W_{hyst}(J_p, J_b)$

Let us consider the SPM and the irreversible part of the density function $p_{irr}(\alpha,\beta) = (1/J_s)\cdot\varphi(\alpha)\varphi(-\beta)$, according to the factorization property (1). The identification of $p_{irr}(\alpha, \beta)$ is the key step of the SPM, requiring pre-emptive measurements. A simple approach consists in measuring the ascending (or descending) branch of the limit cycle (for example, the return curve from J_p = - 1.6 T in non-oriented Fe-(3 wt%)Si sheets). We express then the magnetization attained under the effective quasi-static field H along the major ascending curve by the SPM integral

$$J_{\uparrow}(H) = J(-H_{\mathrm{s}}) + 2\int_{-H_{\mathrm{s}}}^{H}\varphi(\alpha)\mathrm{d}\alpha\int_{-H_{\mathrm{s}}}^{\alpha}\varphi(-\beta)\mathrm{d}\beta + \int_{-H_{\mathrm{s}}}^{H}\mu_{\mathrm{rev}}(\alpha)\mathrm{d}\alpha\,, \qquad (18)$$

where $-H_s = -\alpha_{lim} = -\beta_{lim}$ is the field at technical saturation. An analogous equation is obtained for the descending limit

branch. With the symbols ↑ and ↓ we denote the ascending and descending loop branches, respectively. In Appendix B we demonstrate that, starting from (18), the distribution function $\varphi(H)$ and its primitive $\Phi(H)$ can be explicitly related to $J_{\uparrow}(H)$, its derivative $\mathrm{d}J_{\uparrow}(H)/\mathrm{d}H$, and the reversible permeability $\mu_{\mathrm{rev}}(H)$ pertaining to the limit major loop. Posing for simplicity $\Phi(H_s) = 0$, we get from (18)

$$\mathrm{d}J_{\uparrow}(H)/\mathrm{d}H = -2(\tfrac{\mathrm{d}\Phi(H)}{\mathrm{d}H})\Phi(-H) + \mu_{\mathrm{rev}}(H) \qquad (19)$$

$$J_{\uparrow}(H) + J_{\uparrow}(-H) = -2\,\Phi(H)\cdot\Phi(-H)\,, \qquad (20)$$

which combine to provide the solution for the primitive associated with a given effective quasi-static field H_{stat}

$$\Phi(H_{\mathrm{stat}}) = -\sqrt{J_{\downarrow}(H=0)}\,\exp\Big(\int_0^{H_{\mathrm{stat}}} \frac{\frac{\mathrm{d}J_{\uparrow}}{\mathrm{d}H} - \mu_{\mathrm{rev}}(H)}{J_{\uparrow}(H)+J_{\uparrow}(-H)}\,dH\Big)\,, \qquad (21)$$

where $J_{\downarrow}(H = 0) = -J_{\uparrow}(H = 0)$ is the polarization along the descending branch of the major loop. The distribution function is then obtained as $\varphi(H_{\mathrm{stat}}) = \mathrm{d}\Phi/\mathrm{d}H_{\mathrm{stat}}$.

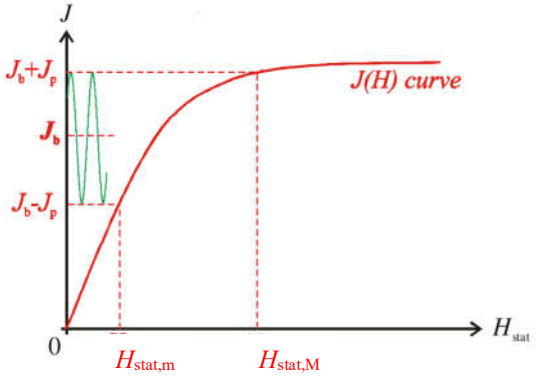

Fig. 5. Determination on the anhysteretic curve of the fields $H_{\mathrm{stat,m}}$ and $H_{\mathrm{stat,M}}$ corresponding to the biased polarization values J_b-J_p, and J_b+J_p.

Let us then discuss how to predict the area of a quasi-static loop of peak-to-peak amplitude $2J_p$ with polarization oscillating between J_b-J_p and J_b+J_p around the bias J_b (see Fig. 2). Let $H_{\mathrm{stat,m}}$ and $H_{\mathrm{stat,M}}$ be the static field values corresponding to the polarization levels J_b-J_p and J_b+J_p. They are not univocally identified, unless the previous magnetic history is known. In such a case, a numerical inversion of the SPM is required. To simplify the matter, at the cost of a certain degree of approximation, we identify $H_{\mathrm{stat,m}}$ and $H_{\mathrm{stat,M}}$ on the easily inverted anhysteretic curve, taken as the curve bisecting the limit cycle (see Fig. 5).

The area of the biased quasi-static hysteresis loop is given by the integral

$$W_{\mathrm{hyst}}(J_p,J_b) = \oint_{\mathrm{cycle}} H_{\mathrm{stat}}\,dJ_{\mathrm{irr}} = \int_{H_{\mathrm{stat,m}}}^{H_{\mathrm{stat,M}}} H_{\mathrm{stat}}(\mathrm{d}J_{\mathrm{irr}\uparrow}/\mathrm{d}H_{\mathrm{stat}} - \mathrm{d}J_{\mathrm{irr}\downarrow}/\mathrm{d}H_{\mathrm{stat}})\,\mathrm{d}H_{\mathrm{stat}}\,. \qquad (22)$$

From (18), we obtain

$$\frac{\mathrm{d}J_{\mathrm{irr}\uparrow}}{\mathrm{d}H_{\mathrm{stat}}} = 2\,\varphi(H_{\mathrm{stat}})[\Phi(H_{\mathrm{stat,m}}) - \Phi(-H_{\mathrm{stat}})] \qquad (23)$$

and similarly for the descending branch

$$\frac{\mathrm{d}J_{\mathrm{irr}\downarrow}}{\mathrm{d}H_{\mathrm{stat}}} = 2\,\varphi(-H_{\mathrm{stat}})[\Phi(H_{\mathrm{stat,M}}) - \Phi(H_{\mathrm{stat}})], \qquad (24)$$

to finally achieve by (22)

$$W_{\mathrm{hyst}}(J_p,J_b) = 2\int_{H_{\mathrm{stat,m}}}^{H_{\mathrm{stat,M}}} H_{\mathrm{stat}}\{\varphi(H_{\mathrm{stat}})[\Phi(-H_{\mathrm{stat,m}})\Phi(-H_{\mathrm{stat}})] - \varphi(-H_{\mathrm{stat}})[\Phi(H_{\mathrm{stat,M}}) - \Phi(H_{\mathrm{stat}})]\}\,\mathrm{d}H_{\mathrm{stat}}. \qquad (25)$$

By retrieving from the experimental major loop the primitive $\Phi(H_{\mathrm{stat}})$ and the distribution $\varphi(H_{\mathrm{stat}}) = \mathrm{d}\Phi/\mathrm{d}H_{\mathrm{stat}}$, we are then able to calculate by (25) the area $W_{\mathrm{hyst}}(J_p,J_b)$ of the biased quasi-static hysteresis loop.

2.5. *The excess loss W_{exc} and the parameter $V_0(J_p,J_b)$*

We have previously obtained by (13) the excess field

$$H_{\mathrm{exc}}(t) = H(t) - H_{\mathrm{stat}}(t) = \frac{4}{3}\frac{sign(\mathrm{d}H_{\mathrm{stat}}/\mathrm{d}t)}{\sqrt{k_{\mathrm{d}}}}\sqrt{\left|\frac{\mathrm{d}H_{\mathrm{stat}}}{\mathrm{d}t}\right|}\,, \qquad (26)$$

as the difference between the effective dynamic field $H(t)$, as given by (5), and the static field at the same magnetization value (see Fig. 2). The excess energy loss, expressed in [J/m^3], is calculated by the time integral

$$W_{\mathrm{exc}} = \int_0^{1/f} H_{\mathrm{exc}}\frac{\mathrm{d}J}{\mathrm{d}t} = \frac{4}{3\sqrt{k_{\mathrm{d}}}}\int_0^{1/f}\sqrt{\frac{dH_{\mathrm{stat}}}{\mathrm{d}J}}\left|\frac{\mathrm{d}J}{\mathrm{d}t}\right|^{3/2}\mathrm{d}t \qquad (27)$$

But, according to (4), W_{exc} can also be written as

$$W_{\mathrm{exc}}(f) = \sqrt{\sigma G S V_0(J_p,J_b)}\int_0^{1/f}\left|\frac{\mathrm{d}J}{\mathrm{d}t}\right|^{3/2}\mathrm{d}t. \qquad (28)$$

The parameter $V_0(J_p,J_b)$ is independent of the specific flux waveform and we can simplify the matter by assuming $\left|\frac{\mathrm{d}J}{\mathrm{d}t}\right| = 4J_p f$, constant across the $\pm J_p$ loop (triangular $J(t)$). By equating (27) and (28), we get

$$V_0(J_p,J_b) = \frac{16}{9}\frac{1}{\sigma G S}\frac{1}{k_{\mathrm{d}}}\left[f\int_0^{1/f}\sqrt{\left(\frac{\mathrm{d}H_{\mathrm{stat}}}{\mathrm{d}J}\right)_{\mathrm{TRI}}}\,\mathrm{d}t\right]^2 \qquad (29)$$

where the subscript TRI stands for triangular polarization and the integrand contains the dependence of V_0 on J_p and J_b. By decomposing the hysteresis cycle into its ascending and descending branches and posing

$$\mathrm{d}t = \frac{\mathrm{d}J/\mathrm{d}H_{\mathrm{stat}}}{|\mathrm{d}J/\mathrm{d}t|}\cdot\mathrm{d}H_{\mathrm{stat}} = \frac{\mathrm{d}J/\mathrm{d}H_{\mathrm{stat}}}{4J_p f}\cdot\mathrm{d}H_{\mathrm{stat}}\,, \qquad (30)$$

we obtain from (29), using (23) and (24) and including the contribution of the reversible permeability μ_{rev} to $\left|\frac{\mathrm{d}J}{\mathrm{d}t}\right|$,

$$V_0(J_p, J_b) = \frac{1}{9\sigma G S k_d J_p^2}\left(\int_{H_{stat,m}}^{H_{stat,M}} \Im_0(H_{stat})\,\mathrm{d}\,H_{stat}\right)^2, \qquad (31)$$

with

$$\Im_0(H_{stat}) = \sqrt{2\varphi(H_{stat})\left[\Phi(-H_{stat}) - \Phi(-H_{stat,m})\right] + \mu_{rev}(H_{stat})} + \sqrt{2\varphi(-H_{stat})\left[\Phi(H_{stat}) - \Phi(H_{stat,M})\right] + \mu_{rev}(H_{stat})} \qquad (32)$$

We thus arrive at the functional dependence of the bias-affected parameter $V_0(J_p, J_b)$ on the SPM parameters Φ, $H_{stat,m}$, $H_{stat,M}$, μ_{rev}, k_d and we can calculate $W_{exc}(J_p, J_b, f)$ by (27), whatever the flux waveform. It is remarked that in a number of cases one can approximate the branch of the quasi-static major loop by a hyperbolic tangent function. For the ascending branch, we write

$$J_{\uparrow}(H_{stat}) = A \tanh\frac{H_{stat} - H_c}{\zeta H_c} + \int_{-H_s}^{H_{stat}} \mu_{rev}(H)\mathrm{d}H\,, \qquad (33)$$

where H_c is the coercive field and A and ζ are fitting parameters. Use of (33) permits one to derive $\Phi(H_{stat})$ and $\varphi(H_{stat})$ as closed expressions.

We finally stress that the previous equations have general value and always apply, with and without bias.

3. Experimental method and procedure

In the previous Section 2 we have demonstrated how the magnetic energy loss in magnetic steels can be predicted as a function of frequency in the presence of a DC bias by connecting and implementing the Static Preisach Model and the concept of loss separation in the framework of the Statistical Theory of Losses. A synthetic view of the procedure devised for the calculation of $W(J_p, J_b, f)$ is provided in the flow chart shown in Fig. 6. We discuss now the loss measurements performed on a variety on non-oriented and grain-oriented alloys and their comparison with the model predictions.

3.1 Measurement method

Magnetic energy losses were measured, with and without DC bias, on a grain-oriented and two non-oriented Fe-Si steel sheets, and on an Fe-Co sheet. The physical parameters of the investigated materials are listed in Table I. The measurements were performed, according to the standards, on Epstein strip samples, using a 700-turn frame below f = 400 Hz and a 200-turn frame above such a frequency. A calibrated broadband hysteresisgraph/wattmeter, endowed with digital control of the sinusoidal induction waveform [43] and making use of a 12-bit LeCroy HDO 4054A oscilloscope for signal acquisition and A/D conversion, was employed. With the frequency ranging between 1 Hz and 1 kHz, energy loss measurements with zero bias for different J_p values were first performed. For each material, the limit quasi-static major cycle (the one depleting or nearly depleting at peak value the domain wall processes) was also measured. The return curve of this cycle was associated with (18) and used to identify the irreversible Preisach Distribution Function, according to the procedure described in Appendix B. The loss measurements versus

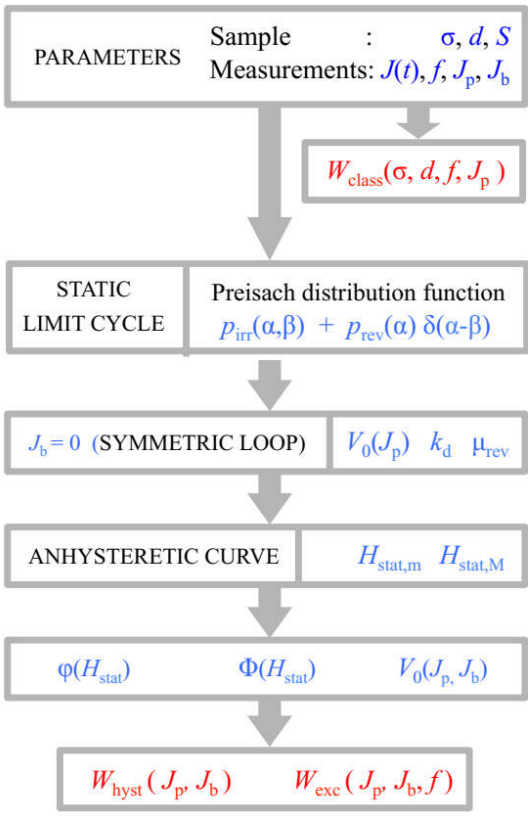

Fig. 6. Flow-chart describing the calculation of the energy loss components at the frequency f in a steel sheet subjected to DC-bias. σ, d, and S are conductivity, thickness, and cross-sectional area of the sheet sample, respectively. J_b is the bias polarization value. The peak-to-peak polarization swing is $2J_p$.

ss

frequency were then repeated, after imposing the polarization bias J_b. A fixed value $J_p = \pm 0.5$ T for the peak polarization of the biased loop was chosen, with J_b values ranging between 0.5 T and 1.5 T. Fig. 7 provides a schematic view of the method devised for the reproducible measurement of the energy loss under defined polarization bias. This follows from the necessity of unambiguously identifying the biased hysteresis loop, in compliance with the non-local memory property of magnetic hysteresis. After low-frequency demagnetization, a major loop with symmetrically nested minor loops having the desired amplitude $\pm J_p$ and bias polarization $\pm J_b$ are obtained by imposing via feedback the polarization waveform shown in Fig. 7a. A sequence of n nested biased loops are made at the frequency f for any given pair (J_p, J_b), in order to reach the steady state. It is n = 5 in the example provided in Fig. 7a, corresponding to a major loop run at the frequency $f_0 = f / 2n$. The case of a measurement made at f = 50 Hz (f_0 = 5 Hz) in the 0.345 mm thick non-oriented Fe-Si sheet is shown in Fig. 7b, where J_p = 0.5 T and J_p = 0.75 T. It is outlined in the same figure that the measured DC-biased cycle is the one occurring at the end of each half-period of the main cycle.

TABLE I
PHYSICAL PROPERTIES OF THE INVESTIGATED STEEL SHEETS

STEEL SHEET	d (mm)	δ (kg/m^3)	σ (Ω^{-1}m^{-1})	J_s (T)	$<s>$ μm
NO Fe-(3.5%)Si	0.345	7600	$1.77\cdot10^6$	1.98	200
NO Fe-(3.2%)Si	0.194	7650	$1.92\cdot10^6$	2.0	122
GO Fe-(3 %)Si	0.280	7650	$2.08\cdot10^6$	2.02	8500
$Fe_{49}Co_{49}V_2$	0.201	8120	$2.27\cdot10^6$	2.33	56

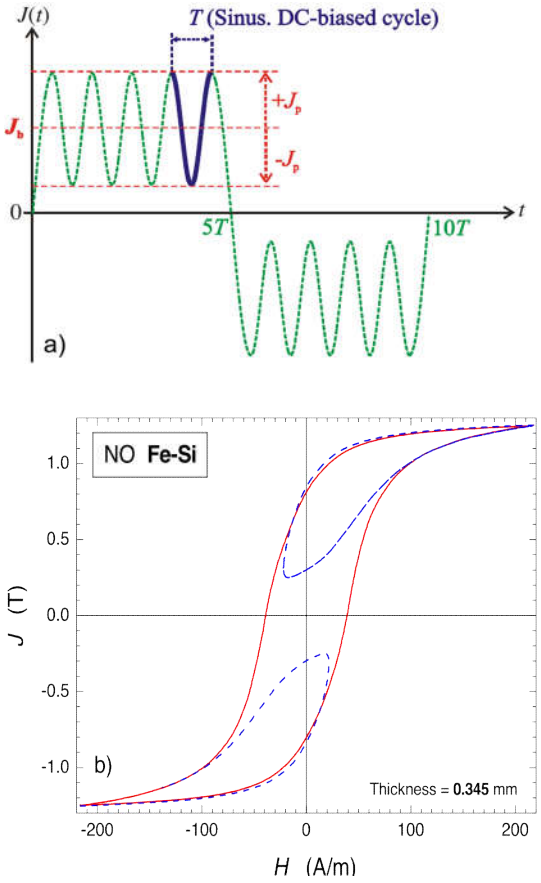

Fig. 7. a) The hysteresis loops of peak amplitude $\pm J_p$ are measured around the polarization bias J_b as minor loops symmetrically nested into a major loop, as shown for a non-oriented Fe-Si 0.345 mm thick sheet sample in b). The biased loops are obtained in this case at the frequency f = 50 Hz, with J_b = 0.75 T and J_p = 0.5 T. The frequency of the major loop is f/10 = 5 Hz.

3.2 *Unbiased (J_b = 0) hysteresis loops.*

The previously formulated expressions for $W_{hyst}(J_p, J_b)$ and $W_{exc}(J_p, J_b, f)$, besides the obvious contribution (3) of the classical loss $W_{class}(J_p, f)$, apply in a simplified way to the limiting case of unbiased polarization, where we shall find $W_{hyst}(J_p)$ by (25) and the quantity $V_0(J_p)$ (and eventually $W_{exc}(J_p, f)$ by (31) and (32). But, as previously stressed, the unbiased condition can be simply and alternatively treated according to the standard loss separation, directly providing at all frequencies $W_{class}(J_p, f)$ (by (3)), $W_{hyst}(J_p)$ (by extrapolating the loss $W(J_p, f)$ measured at two different frequencies to f = 0), and $W_{exc}(J_p, f)$ (by subtracting $W_{class}(J_p, f)$ and $W_{hyst}(J_p)$ from the measured loss $W(J_p, f)$. A comparison can then be made between the results provided by the two different approaches, so as to attain a preliminary validation of the model. *Our final aim is one of predicting the energy loss $W(J_p, J_b, f)$, under whatever polarization bias J_p, making use of the simple STL analysis of the unbiased one $W(J_p, f)$.*

In order to calculate $W_{hyst}(J_p)$ by (25) and $W_{exc}(J_p)$ by (31) and (32), we need to determine the Preisach distribution function $\varphi(H_{stat})$, its primitive $\Phi(H_{stat})$, and the dynamic constant k_d. Such a constant, related to the average range of the mesoscopic regions reversing in a correlated fashion (Barkhausen reversals), is approximated by (17). However, we determine it here, for the sake of comparison, using the standard DPM approach [44], where we calculate a few symmetric dynamic cycles under imposed sinusoidal induction up to 400 Hz and we adjust the value of k_d for best fitting. For the calculation of the integrals (25) and (31), taken between symmetric limits, we make use, at the cost of a certain approximation, of the analytical expression (33), fitting the ascending branch of the limit experimental cycle. This is measured between ± 1.5 T in NO Fe-Si, ± 1.75 T in GO Fe-Si, and ± 2.1 T in the Fe-Co sheets. We write (33) as

$$J_{\uparrow}(H_{stat}) = A \cdot \tanh \frac{H_{stat} - H_c}{\zeta\, H_c} + \mu_{rev} H_{stat}, \qquad (34)$$

by substituting $\int_{-H_s}^{H_{stat}} \mu_{rev}(H)\mathrm{d}H$ with $\mu_{rev} H_{stat}$ and taking an appropriate value for μ_{rev} (see Table II). This approximation is justified considering the minor played by the reversible processes along the required limit cycle. By using the simplifying notation ξ=1/ζ, we obtain

$$\Phi(H_{stat}) = -\frac{\sqrt{A \sinh \xi \cosh \xi}}{\cosh\left(\xi \frac{H_{stat} - H_c}{H_c}\right)} \exp\left(-\xi \frac{H_{stat}}{H_c} \coth 2\xi\right) \qquad (35)$$

$$\varphi(H_{stat}) = \frac{\xi}{H_c \sinh 2\xi} \frac{\cosh(\xi(H_{stat}/H_c+1))}{\cosh(\xi(H_{stat}/H_c-1))} \Phi(H_{stat}), \qquad (36)$$

with the parameters A, ζ, and H_c in (34) obtained by best fitting of the major loop. These parameters are listed in Table II. We then calculate $W_{hyst}(J_p)$ by (25) and $W_{exc}(J_p)$ by (28) – (32), applying these equations to the limiting case of *unbiased loops* of peak value J_p. The so-obtained $W_{hyst}(J_p)$ behaviors are compared in all the investigated materials with the same quantity resulting from the standard loss separation procedure. Two examples of such comparisons are given in Fig. 8

TABLE II
FITTING PARAMETERS OF THE LIMIT HYSTERESIS CYCLE (34)

STEEL SHEET	A (T)	H_c (A/m)	ζ	μ_{rev}/μ_0	k_d (m/As)
NO Fe-(3.5%)Si	1.34	28.0	1.2	120	350
NO Fe-(3.2%)Si	1.33	39.4	1.1	150	1200
GO Fe-(3 %)Si	1.87	6.8	0.5	200	57
$Fe_{49}Co_{49}V_2$	2.29	31	0.324	400	1100

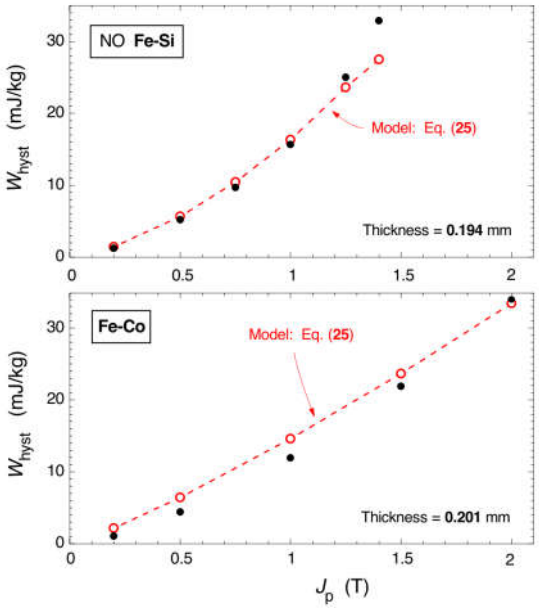

Fig. 8. Example of hysteresis loss component $W_{hyst}(J_p)$, obtained in Fe-Si and Fe-Co non-oriented steel sheets by extrapolating the energy loss $W(f)$, measured in the *absence of polarization bias*, to $f \rightarrow 0$ (solid symbols). The dashed lines are obtained by predicting $W_{hyst}(J_p)$ by (25), where the Preisach distribution function $\varphi(H_{stat})$ and its primitive are $\Phi(H_{stat})$ are analytically derived, according to (35) and (36).

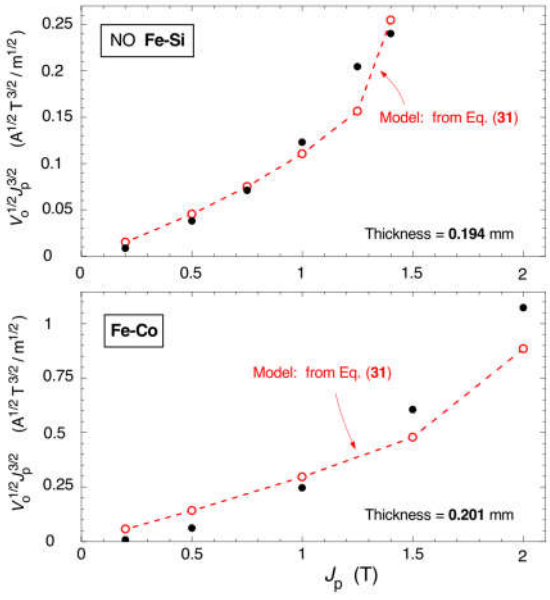

Fig. 9. The quantity $V_0^{1/2}J_p^{3/2}$, which identifies the excess loss component, independent of its frequency behavior, is obtained, for unbiased sinusoidal polarization, applying (37), according to the standard loss separation procedure (solid symbols), and (31) (open symbols and line),through use of (35) and (36).

The expression for the excess loss under sinusoidal unbiased polarization is obtained from (4) as

$$W_{exc}(J_p) = 8.76\sqrt{\sigma GSf}\,(V_0^{1/2}J_p^{3/2}) \quad , \quad (37)$$

which accurately fits, within the upper frequency limit imposed by the skin effect, the experimental excess loss behavior [31]. This equation shows that the dependence of W_{exc} on the material microstructure identifies with that of the parameter $V_0(J_p)$. We show then in Fig. 9 the evolution of the quantity $V_0^{1/2}J_p^{3/2}$ versus J_p obtained by (37) upon loss separation in the investigated steel sheets (solid symbols). The same quantity, calculated with (31) via the Preisach function (36) and its primitive (35) and the dynamic constant k_d obtained by the previously described DPM approach, is shown to satisfactorily compare with the results of (37).

3.3 Biased ($J_b > 0$) hysteresis loops.

Having verified and validated the outcome of the model under the unbiased exciting regimes, we proceed to its full application to the DC-biased hysteresis loops and the frequency dependence of the energy loss $W(J_p, J_b, f)$ in the investigated NO and GO steel sheets and the Fe-Co alloy. We start by making the previously described comparison between the behaviors of the $V_0^{1/2}J_p^{3/2}$ predicted in the absence of bias and shown in Fig. 9. We now avoid, however, the complications of the DPM and we determine the dynamic constant k_d in (31) by adjusting its value for closest

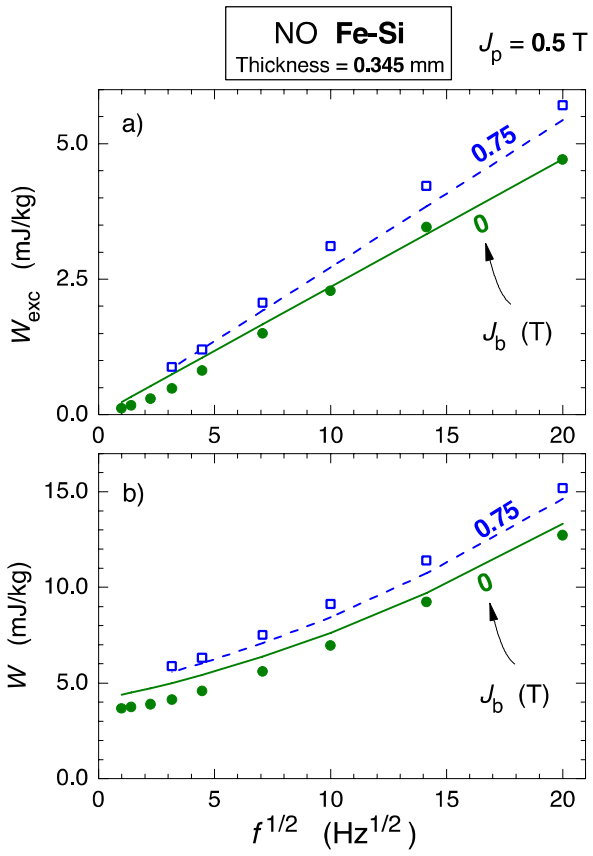

Fig. 10. Non-oriented Fe-(3.5%)Si 0.345 mm thick sheet and its energy loss behavior with $J_p = \pm 0.5$ T up to 400 Hz under unbiased and biased ($J_b = 0.75$ T) sinusoidal polarization Symbols: measurements. Lines: model prediction. a) Excess loss component $W_{exc}(J_p, J_b, f)$. b) Total loss $W(J_p, J_b, f)$.

comparison between the results provided by the conventional loss decomposition (unbiased polarization) using the STL (solid symbols in Fig. 9) and the outcome of (31). Table II provides the so-calculated k_d values for all the investigated materials. It is remarked that k_d is around one order of magnitude lower in the GO sheets than in the NO ones. This is consistent with the idea that broader domain structures imply larger contribution of any single magnetic object to the global flux rate of change and ensuing larger associated dynamic field, according to the approximate expression provided by (17).

With $\varphi(H_{stat})$, $\Phi(H_{stat})$, and k_d determined following the previous procedure, we calculate $W_{hyst}(J_p, J_b)$ and $W_{exc}(J_p, J_b, f)$ by (25) and (28) and add these quantities to the bias-independent classical component $W_{class}(J_p)$, given by (3), to

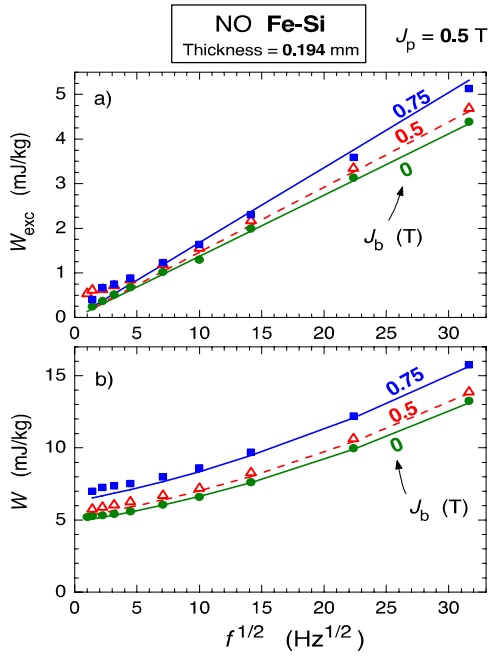

Fig. 11. Non-oriented Fe-(3.%)Si 0.194 mm thick sheet and its energy loss behavior with J_p = 0.5 T up to 1 kHz under unbiased and biased (J_b = 0.5 T, 0.75 T) sinusoidal polarization Symbols: measurements. Lines: model prediction. a) Excess loss component $W_{exc}(J_p, J_b, f)$. b) Total loss $W(J_p, J_b, f)$.

TABLE III
MEASURED AND PREDICTED HYSTERESIS LOSS COMPONENT $W_{hyst}(J_p, J_b)$ AT J_p = 0.5 T

STEEL SHEET	d (mm)	J_b (T)	W_{hyst} (mJ/kg) Measured	Predicted
NO Fe-(3.5%)Si	0.345	0	3.64	4.15
		0.75	4.88	4.59
NO Fe-(3.2%)Si	0.194	0	4.67	4.87
		0.5	5.49	5.16
		0.75	6.57	6.28
GO Fe-(3 %)Si	0.280	0	0.395	0.454
		0.75	0.418	0.515
		1.2	1.215	1.311
$Fe_{49}Co_{49}V_2$	0.201	0	4.39	4.62
		1.5	4.47	5.09

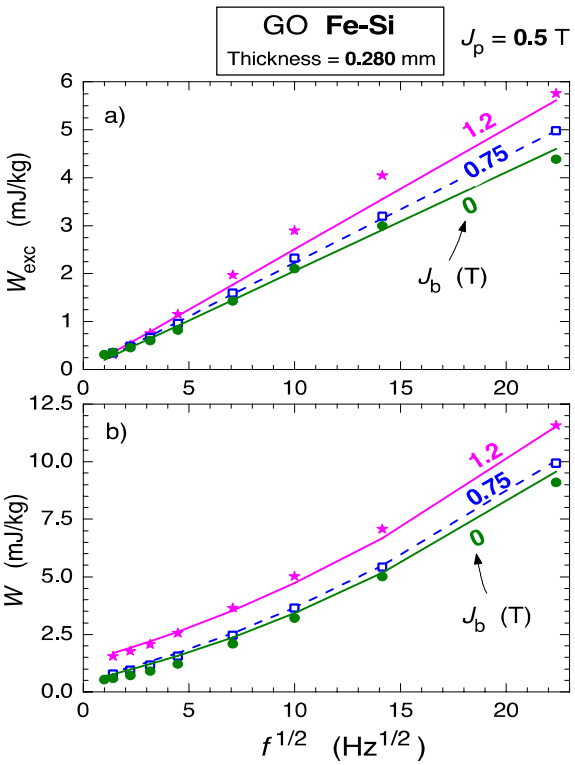

Fig.12. Grain-oriented Fe-(3%)Si 0.280 mm thick sheet and its energy loss behavior with J_p = 0.5 T up to 500 Hz under unbiased and biased (J_b = 0.75 T, 1.2 T) sinusoidal polarization Symbols: measurements. Lines: model prediction. a) Excess loss component $W_{exc}(J_p, J_b, f)$. b) Total loss $W(J_p, J_b, f)$.

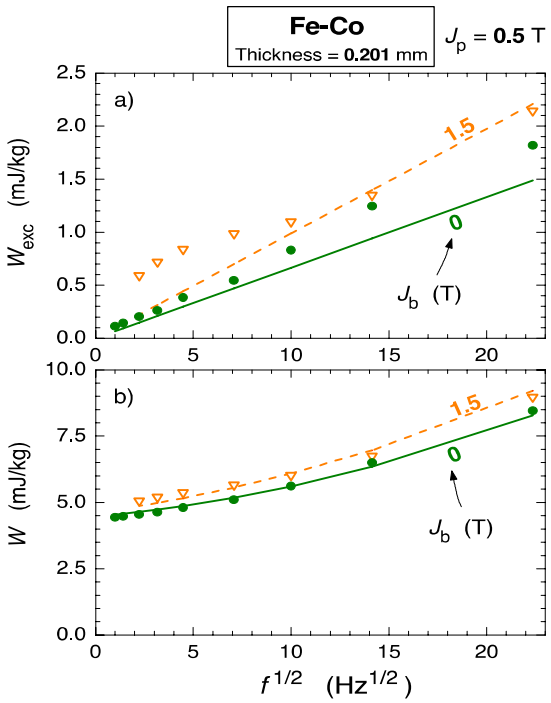

Fig.13. Non-oriented $Fe_{49}Co_{49}V_2$ 0.201 mm thick sheet and its energy loss behavior with J_p = 0.5 T up to 500 Hz under unbiased and biased (J_b = 1.5 T) sinusoidal polarization Symbols: measurements. Lines: model prediction. a) Excess loss component $W_{exc}(J_p, J_b, f)$. b) Total loss $W(J_p, J_b, f)$.

finally obtain the frequency dependence of the total energy loss $W(J_p, J_b, f)$. Figs. 10 – 13 show measured and predicted $W(J_p, J_b, f)$ behaviors in the investigated materials for a defined polarization swing $2J_p$ = 1.0 T and bias values J_b ranging between 0.5 T and 1.5 T. The predicted hysteresis losses $W_{hyst}(J_p, J_b)$ are compared with the calculated ones in Table III. Some discrepancies occurring between measurement and prediction descend from certain limits of the analytical approach, namely the description of the reverse branch of the limit cycle by (34). We see, however, in Figs. 11-13 and in Table IV that the eventually predicted total losses $W(J_p, J_b, f)$ at power frequencies and beyond become, with and without bias, close to the experimental values. We observe, in particular, that the model brings to light the role of the excess losses in the increase of the measured loss $W(J_p, J_b, f)$ with increasing J_b. Physically, this is interpreted in terms of a corresponding evolution of $V_0(J_p, J_b)$, the parameter directly related to the distribution of the local coercive fields, which inevitably increases when the material is brought towards higher induction values, that is, increasingly harder magnetization processes.

TABLE IV
MEASURED AND PREDICTED ENERGY LOSS
AT J_p = 0.5 T AND f = 100 Hz

STEEL SHEET	d (mm)	J_b (T)	W (mJ/kg) Measured	Predicted
NO Fe-(3.5%)Si	0.345	0	6.92	7.62
		0.75	9.12	8.44
NO Fe-(3.2%)Si	0.194	0	6.61	6.63
		0.5	7.18	7.02
		0.75	8.60	8.35
GO Fe-(3 %)Si	0.280	0	3.21	3.42
		0.75	3.64	3.05
		1.2	5.02	4.12
$Fe_{49}Co_{49}V_2$	0.201	0	5.61	5.60
		1.5	6.02	5.84

5. Conclusion

The frequency dependence of the magnetic energy losses in steel sheets subjected to a DC field bias is theoretically assessed by analytical formulations and experimentally verified in a number of non-oriented and grain-oriented alloys. The here discussed model overcomes the limitations of the nowadays prevalent empirical approaches, like the popular models based on the Steinmetz's law, whose feeble connection with the physical properties of the magnetization process is a main limiting factor in applications. In these models, in particular, the quasi-static loss is generally credited with the whole increase of the loss under DC field bias. However, even a qualitative analysis of the magnetization process makes clear that coercivity and dynamics of the domain walls are correlated. This conclusion is quantitatively assessed by the Statistical Theory of Losses and the Dynamic Preisach Model. We show in this paper that, starting from the conceptual framework of the Dynamic Preisach Model, we can arrive at a theoretical formulation of the energy loss and its dependence on frequency, which is valid with and without DC-bias. An analytical relationship between the dynamic and quasi-static effective fields is obtained, by which the Dynamic Preisach Model can be connected to the easily afforded Static Preisach Model. This brings to light, in particular, the role of the bias field on the excess loss component, which can be accounted for by making general the formula of the excess loss component provided by the Statistical Theory of Losses. Implementation of the model requires a minimum set of pre-emptive experimental data, namely a major (limit) DC hysteresis loop and a couple of energy loss values at two different frequencies under unbiased conditions, over a reasonable range of peak polarization values. The increase of the measured loss with the bias is justified and ultimately related to the distribution of the local coercive fields and the portion of it associated with higher fields, widening under increasing bias.

The experiments performed for different values of the bias polarization on different types of steel sheets demonstrate the increase of the dynamic loss with biasing and the ability of the model to quantitatively account for such an effect.

References

[1] S. Maniktala, *Switching Power Supply Design & Optimization*. New York, NY, USA: McGraw-Hill, May 2004.

[2] G. Di Capua and N. Femia, "A novel method to predict the real operation of ferrite Inductors with moderate saturation in switching power supply," *IEEE Trans. Power. Electron.*, vol. 31, no. 3, pp. 2456-2564, March 2016. doi: 10.1109/TPEL.2015.2438952.

[3] A. Hilal, M.A. Raulet, C. Martin, and F. Sixdenier, "Power loss prediction and precise modeling of magnetic powder components in DC–DC power converter application," *IEEE Trans. Power Electron*. Vol. 30, no. 4, pp, 2232-2238, April 2015. doi: 10.1109/TPEL.2014.2330952.

[4] H. Kosai, Z. Turgut, and J. Scofield, "Experimental investigation of DC-bias related core losses in a boost inductor,"*IEEE Trans. Magn.*, vol. 49, no. 7, pp. 4168-4171, July 2013, doi: 10.1109/TMAG.2013.22442863.

[5] X. Li, X. Wen, P.N. Markham, and Y. Liu, "Analysis of nonlinear characteristics for a three-phase, five-limb transformer under DC bias," *IEEE Trans. Power Del.* vol. 25, no. 4, pp. 2504-2510, Oct. 2010, doi: 10.1109/TPWRD.2010.2052837.

[6] S. Zhu and M. Cheng, "Core loss analysis and calculation of stator permanent-magnet machine considering DC-biased magnetic induction," *IEEE Trans. Ind. Electron.*, vol. 61, no. 10, pp. 5203–5212, Oct. 2014, doi:10.1109/TIE.2014.2300062

[7] K. Atallah, D. Howe, P. H. Mellor, and D. A. Stone, "Rotor loss in permanent-magnet brushless AC machines," *IEEE Trans. Ind. Appl.*, vol. 36, no. 6, pp. 1612–1618, Nov./Dec. 2000, doi:10.1109/28.887213.

[8] Y. Liao, F. Liang, and T.A. Lipo, "A novel permanent magnet motor with doubly salient structure," *IEEE Trans. Ind. Appl.* , vol. 31, no. 5, pp. 1069-1078, Sep.-Oct. 1995. doi: 10.1109/28.464521.

[9] W. Hua, X. Yin, G. Zhang, and M. Cheng, "Analysis of two novel five-phase hybrid-excitation flux-switching machines for electric vehicles," *IEEE Trans. Magn.*, vol. 50, no. 11, Art. no. 8700305, Nov. 2014. doi:10.1109/TMAG.2014.2323089.

[10] A. Boglietti, A. Cavagnino, D.M. Ionel, M. Popescu, D.A. Staton, and S. Vaschetto, "A General Model to Predict the Iron Losses in PWM Inverter-Fed Induction Motors," *IEEE Trans. Ind. Appl.* , vol. 46, no. 5, pp. 1882-1890, Sep.-Oct. 2010. doi: 10.1109/TIA.2010.2057393.

[11] P. Rasilo, W.Martinez, K. Fujisaki,J. Kyyra, and A. Ruderman, "Simulink model for PWM-supplied laminated magnetic cores including hysteresis, eddy-current, and excess losses," *IEEE Trans. Power Electron*. Vol. 34, no. 2, pp, 1683-1695, Febr. 2019. doi: 10.1109/TPEL.2018.2835661.

[12] G. Bertotti, *Hysteresis in Magnetism,* San Diego, CA, USA: Academic Press, 1998, p. 433.

[13] I.D. Mayergoyz, *Mathematical models of Hysteresis and their Applications*, New York, NY, USA: Elsevier, 2003.

[14] T. V. Tran, F. Moussouni, S. Brisset, and P. Brochet, "Adapted output space-mapping technique for a bi-objective optimization," *IEEE Trans. Magn.*, vol. 46, no. 8, pp. 2990–2993, Aug. 2010, doi:10.1109/TMAG.2010.2043343.

[15] J. Reinert, A. Brockmeyer, and Rik W.A.A De Donker, "Calculation of losses in ferro and ferrimagnetic materials based on a modified Steinmetz equation," *IEEE Trans. Ind. Appl.* vol. 37, no. 4, pp. 1055-1061, July/Aug. 2001, doi: 10.1109/28.936396.

[16] C. Simao, N. Sadowski, N.J. Batistela, and J.P.A. Bastos, "Evaluation of hysteresis losses in iron sheets under DC-biased inductions," *IEEE Trans. Magn.*, vol. 45, no. 3, pp. 1158-1161, March 2009, doi:10.1109/TMAG.2009.2012663.

[17] J. Mühlethaler, J. Biela, J.W. Kolar, and A. Ecklebe, "Core losses under the DC bias conditionbased on Steinmetz parameters," *IEEE Trans. Power Electron.* vol. 27, no. 2, pp. 953-963, Febr. 2012, doi: 10.1109/TPEL.2011.2160971.

[18] H. Kosai, Z. Turgut, T. Bixel, and J. Scofield, "Performance comparison of Finemet and Metglas tape cores under non-sinusoidal waveforms with DC bias," *IEEE Trans. Magn.*, vol. 52, no. 7, July 2016, Art. no. 8400704, doi: 10.1109/TMAG.2015.2512438.

[19] J. Mülethaler, J. Biela, J.W. Kolar, ans A. Ecklebe, "Improved core loss calculation for magnetic components employed in power electronic systems," *IEEE Trans. Power. Electron.*, vol. 27, no. 2, pp. 964–973, Febr. 2012. doi: 10.1109/TPEL.2011.2162252.

[20] S. Barg, K. Ammous, H. Mejibri, and A. Ammous, "An improved empirical formulation for magnetic core losses estimation under nonsinusoidal induction," *IEEE Trans. Power. Electron.*, vol. 32, no. 3, pp. 2146-2154, March 2017. doi: 10.1109/TPEL.2016.2555359.

[21] G. Bertotti, "General properties of power losses in soft ferromagnetic materials," *IEEE Trans. Magn.*, vol. 24, no. 1, pp. 621-630, Jan. 1988. doi: 10.1109/20.43994.

[22] S. Zhu, M. Cheng, J. Dong, and J. Du, "Core loss analysis and calculation of stator permanent-magnet machine considering DC-biased magnetic induction ," *IEEE Trans. Ind. Electron*., vol. 61, no. 10, pp. 5203–5212, Oct. 2014, doi: 10.1109/TIE.2014.2300062.

[23] Z.Q. Zhu. SD, Xue, W.Q. Chu, J. Feng, S. Guo, Z. Chen, and J. Peng, "Evaluation of iron loss models in electrical machines ," *IEEE Trans. Ind. Appl*., Nov. 2018, doi: 10.1109/TIA.2018.2880674.

[24] Y.Wang and Z. Liu, "Estimation model of core loss under DC bias," *IEEE Trans. Appl. Supercond*., vol. 26, no. 7, Art. no. 0608905, Oct. 2016, doi: 10.1109/TASC.2016.2594806.

[25] V. Basso and G. Bertotti, "Description of magnetic interaction and Henkel plots by the Preisach hysteresis model," *IEEE Trans. Magn.*, vol. 30, no. 1, pp. 64-72, Jan. 1994. doi: 10.1109/20.272516.

[26] V. Basso, "Hysteresis models for magnetization by domain wall motion," *IEEE Trans. Magn.*, vol. 34, no. 4, pp. 2207-2212, July 1998. doi: 10.1109/20.703857.

[27] G. Bertotti, "Generalized Preisach model for the description of hysteresis and eddy current effects in metallic ferromagnetic materials," *J. Appl. Phys.,* vol. 69, no. 8, pp. 4608-4610, Apr. 1991. doi:10.1063/1.348325.

[28] G. Bertotti, "Dynamic generalization of the scalar Preisach model of hysteresis," *IEEE Trans. Magn.*, vol. 28, no. 5, pp. 2599–2601, Sep. 1992. doi:10.1109/20.179569.

[29] V. Basso, G. Bertotti, O. Bottauscio, F. Fiorillo, M. Pasquale, M. Chiampi, and M. Repetto., "Power losses in magnetic laminations with hysteresis: finite element modeling and experimental validation," *J. Appl. Phys.* vol. 81, pp. 5606–5608, Apr. 1997, doi:10.1063/1.364614.

[30] E. Barbisio, O. Bottauscio, M. Chiampi, F. Fiorillo, and C. Ragusa, : "Prediction of magnetic power losses in soft laminations under DC-biased supply," *J. Magn. Magn. Mater.*, vol. 290, pp. 1476-1479, 2005, doi: 10.1016/j.jmmm.2004.11.553.

[31] E. Barbisio, F. Fiorillo, and C. Ragusa, "Predicting loss in magnetic steels under arbitrary induction waveform and with minor hysteresis loops," *IEEE Trans. Magn.*, vol. 40, no. 4, pp. 1810-1819, July 2004, doi: 10.1109/TMAG.2004.830510.

[32] C. Beatrice, C. Appino, O. de la Barrière, F. Fiorillo, and C. Ragusa, "Broadband magnetic losses in Fe-Si and Fe-Co laminations," *IEEE Trans. Magn.*, vol. 50, no. 4, Apr. 2014, Art. no. 6300504 , doi: 10.1109/TMAG.2013.2286923

[33] O. de la Barrière, C. Ragusa, C. Appino, and F. Fiorillo, "Prediction of energy losses in soft magnetic materials under arbitrary induction waveform and DC bias," *IEEE Trans. Ind. Electron*., vol. 64, no. 3, pp. 2522–2529, March 2017, doi: 10.1109/TIE.201462608886.

[34] S. Steentjes, S.E. Zirka, Y.I. Moroz, E.Y. Moroz, and K. Hameyer, "Dynamic magnetization model of nonoriented steel sheets," *IEEE Trans. Magn.*, vol. 50, no. 4, 7300204, April 2014, doi: 10.1109/TMAG.2013.2284357.

[35] S. E. Zirka, Y. I. Moroz, S. Steentjes, K. Hameyer, K. Chwastek, S. Zurek, and R.G. Harrison, "Dynamic magnetization models for soft ferromagnetic materials with coarse and fine domain structure," *IJ. Magn. Magn. Mater.,* vol. 394, pp. 229–236, July 2015. doi: 10.1016/j.jmmm.2015.06.082.

[36] R. Kaczmarek, M. Amar and F. Protat, "Iron loss under PWM voltage supply on Epstein frame and in induction motor core," *IEEE Trans.Magn.*, vol. 32, no. 1, pp. 189-194, Jan. 1996. doi: 10.1109/20.477571.

[37] H. Zhao, C. Ragusa, C. Appino, O. de la Barrière, Y. Wang, and F. Fiorillo, "Energy losses in soft magnetic materials under symmetric and asymmetric induction waveforms," *IEEE Trans. Power. Electron.*, vol. 34, no. 3, pp. 2655-2665, March 2019. doi: 10.1109/TPEL.2018.2837657.

[38] C. Appino, M. Khan, O. de la Barriere, C. Ragusa, F. Fiorillo, "Alternating and Rotational Losses Up to Magnetic Saturation in Non-Oriented Steel Sheets," *IEEE Trans. Magn.,* vol. 52, no. 5, Article no. 6301204, May 2016, doi: 10.1109/TMAG.2016.2528338.

[39] M. LoBue, F. Mazaleyrat, and V. Loyau, "Study of magnetic losses in Mn-Zn ferrites under biased and asymmetric excitation waveforms," *IEEE Trans. Magn.* vol. 46, no. 2, pp. 452-454, Febr. 2010. doi: 10.1109/TMAG.2009.2031471.

[40] C. Beatrice, S. Dobák, E. Ferrara, F. Fiorillo, C. Ragusa, J. Füzer, and P. Kollár, "Broadband magnetic losses of nanocrystalline ribbons and powder cores", *J. Magn. Magn. Mater.* vol. 420, pp. 317-323, Dec. 2016. doi: 10.1016/j.jmmm.2016.07.045

[41] C. Ragusa, C. Appino, and F. Fiorillo, "Magnetic losses under two-dimensional flux loci in Fe-Si laminations," *J. Magn. Magn. Mater.* vol. 316, pp. 454–457, 2007. doi: 10.1016//j.jmmm.2007.03.170.

[42] C. Appino, C. Ragusa, and F. Fiorillo, " Can rotational magnetization be theoretically assessed?," *Int. J. Appl. Electromagnetics Mech.* vol. 44, pp. 355–370, 2014. doi: 10.3233/JAE-141798.

[43] F. Fiorillo, "Meaurements of magnetic materials," *Metrologia*, vol. 47, pp. S114-142, March 2010, doi:10.1088/0026-1394/47/2/S11.

[44] L.R. Dupré, O. Bottauscio, M. Chiampi, M. Repetto, and J. Melkebeek, "Modeling of electromagnetic phenomena in soft magnetic materials under unidirectional time periodic flux excitations," *IEEE Trans. Magn.*, vol. 35, no. 5, pp. 4171-4184, Sep. 1999, doi: 10.1109/20.799065.

[45] C. Ragusa, "An analytical method for the identification of the Preisach distribution function", *J. Magn. Magn. Mater.*, vol. 254, pp. 259-261, 2003, doi: 10.1016/S0304-8853(02)00787-4.

Appendix A

We derive here the differential operator ***F*** connecting $H(t)$, the dynamic field defined in (5), and $H_{stat}(t)$, the field that under quasi-static excitation provides the same irreversible polarization value J_{irr}. We do this by operating on the Preisach plane, where we consider, following the scheme of Fig. 4, the evolution of the irreversible magnetization $J_{irr}(H(t))$ along the ascending limit branch under the monotonically increasing field $H(t)$. $H_{stat}(t)$ travels in the wake of $H(t)$, inside the dynamic strip of width ΔH. The state function $\Psi(\alpha,\beta;t)$ associated with the major ascending branch is independent of β and we write, according to (9),

$$J_{irr}(H(t)) = J_s \int_{-\alpha_{lim}}^{\alpha_{lim}} \Psi(\alpha;t)\mathrm{d}\alpha \int_{-\beta_{lim}}^{\alpha} \cdot p_{irr}(\alpha,\beta)\mathrm{d}\beta. \quad (A.1)$$

By defining the quantity

$$\mu^*_{irr}(\alpha) = J_s \int_{-\beta_{lim}}^{\alpha} p_{irr}(\alpha,\beta)\mathrm{d}\beta = \mu_{irr}(\alpha)/2\,, \quad (A.2)$$

where $\mu_{irr}(\alpha)$ is the slope of the magnetization curve under quasi-static conditions, we express the irreversible polarization along the ascending branch at time t as

$$J_{irr}(H(t)) = \int_{-\alpha_{lim}}^{\alpha_{lim}} \mu^*_{irr}(\alpha)\Psi(\alpha;t)\mathrm{d}\alpha \quad (A.3)$$

The scheme in Fig. 4 compares the step-like and the smooth transitions of Ψ between the values ± 1 occurring under static and dynamic excitation, respectively. We equate the magnetization variations $\Delta J_{dyn} = \Delta J_{stat}$ pertaining to the ($H(t)$-ΔH, H) strip under these two conditions. By taking into account that for the static case $\Psi(H_{stat}) = +1$ and $\Psi(H) = -1$, we write

$$\int_{H-\Delta H}^{H} \mu_{irr}(\alpha)\,\Psi(\alpha;t)\mathrm{d}\alpha =$$

$$= \int_{H-\Delta H}^{H_{stat}} \mu_{irr}(\alpha)\,\mathrm{d}\alpha - \int_{H_{stat}}^{H} \mu_{irr}(\alpha)\,\mathrm{d}\alpha \quad (A.4)$$

and the time derivatives of the left and hand right sides as

$$\frac{\mathrm{d}(\Delta J_{dyn})}{\mathrm{d}t} = \mu_{irr}(H)\Psi(H)\frac{\mathrm{d}H}{\mathrm{d}t} - \mu_{irr}(H-\Delta H)\Psi(H-\Delta H)\frac{\mathrm{d}H}{\mathrm{d}t} +$$

$$+ \int_{H-\Delta H}^{H} \mu_{irr}(\alpha)\cdot\left(\frac{\mathrm{d}\Psi}{\mathrm{d}t}\right)\mathrm{d}\alpha \quad (A.5)$$

$$\frac{\mathrm{d}(\Delta J_{stat})}{\mathrm{d}t} = 2\mu_{irr}(H_{stat})\frac{\mathrm{d}H_{stat}}{\mathrm{d}t} - \mu_{irr}(H-\Delta H)\frac{\mathrm{d}H_{stat}}{\mathrm{d}t} - \mu_{irr}(H)\dot{H}\,. \quad (A.6)$$

Since, and the normalized flux rate of the hysteron is, according to (7),

$$\frac{\mathrm{d}\Psi(\alpha;t)}{\mathrm{d}t} = k_d[H(t)\text{-}\alpha], \qquad (H(t) \geq \alpha) \quad (A.7)$$

we obtain from (A.5) and (A.6)

$$\frac{\mathrm{d}H_{stat}}{\mathrm{d}t} = \frac{k_d}{2\mu_{irr}(H_{stat})}\int_{H-\Delta H}^{H} \mu_{irr}(\alpha)[H(t)-\alpha]\mathrm{d}\alpha \quad (A.8)$$

In order to make explicit the relationship (A.8) between $H(t)$ and $H_{stat}(t)$, we make two simplifying assumptions:

1) *$\mu_{irr}(\alpha)$ is uniform across the dynamic strip [H-ΔH, H].* Consequently, (A.4) and (A.8) become

$$\int_{H-\Delta H}^{H}[1+\Psi(\alpha;\,t)]\mathrm{d}\alpha = 2[H_{stat}(t) - H(t) + \Delta H] \quad (A.9)$$

$$\frac{\mathrm{d}H_{stat}}{\mathrm{d}t} = \frac{k_d}{4}\cdot\Delta H^2\,, \quad (A.10)$$

respectively.

2) *The time derivative $\frac{dH}{dt}$ of the magnetic field is locally uniform.* We can then pose $H(t) = H(t_0) + \frac{\mathrm{d}H}{\mathrm{d}t}\cdot(t-t_0)$, with $H(t_0) = \alpha$ in (A.7), to obtain

$$\frac{\mathrm{d}\Psi(\alpha;t)}{\mathrm{d}t} = k_d\frac{\mathrm{d}H}{\mathrm{d}t}\cdot(t-t_0), \quad (A.11)$$

and by integration

$$\Psi(\alpha;t) = \Psi(\alpha;t_0) + k_d\frac{\mathrm{d}H}{\mathrm{d}t}\int_{t_0}^{t}(t'-t_0)\mathrm{d}t' =$$

$$= -1 + \frac{k_d}{2\left(\mathrm{d}H/\mathrm{d}t\right)}[H(t)-\alpha]^2\,, \quad (A.12)$$

being $\Psi(\alpha;\,t_0) = -1$. The dynamic transition of the hysteron, having threshold field α, follows a parabolic law and saturates at the time t_1 ($\Psi(\alpha;\,t_1) = 1$), where $H(t)$ attains the right boundary of the dynamic strip and $H(t_1) - \alpha = \Delta H$. The strip width is then found to depend on the time derivative of the field as

$$\Delta H = sign(\mathrm{d}H_{stat}/\mathrm{d}t)\cdot 2\sqrt{\frac{1}{k_d}\left|\frac{\mathrm{d}H_{stat}}{\mathrm{d}t}\right|} \quad (A.13)$$

and we can express (A.12) as

$$\Psi(\alpha;\mathrm{t}) = -1 + \frac{2}{\Delta H^2}\cdot[H(t)-\alpha]^2. \quad (A.14)$$

By introducing (A.14) in (A.9), we get

$$\Delta H = \frac{3}{2}[H(t) - H_{stat}(t)], \quad (A.15)$$

and from (A.10) we finally obtain the differential equation (12) relating $H_{stat}(t)$ and $H(t)$ via the constant k_d

$$\frac{\mathrm{d}H_{stat}}{\mathrm{d}t} = sign\big(H(t) - H_{stat}(t)\big)\frac{9}{16}k_d[H(t) - H_{stat}(t)]^2 \quad (A.16)$$

It is noted that at very high frequencies the dynamic strip may become too large for satisfying the approximation of uniform $\mu_{irr}(\alpha)$.

Appendix B

We proceed to the identification of the Preisach distribution function for the irreversible magnetization process $J_s \cdot p_{irr}(\alpha,\beta) = \varphi(\alpha)\varphi(-\beta)$ through knowledge of the ascending/descending branches of the major *quasi-static* hysteresis loop, following the approach discussed in [45]. We start by describing the ascending major curve through the appropriate integral on the Preisach plane

$$J_{\uparrow}(H) = J(-H_s) + \\ +2\int_{-H_s}^{H}\varphi(\alpha)\mathrm{d}\alpha\int_{-H_s}^{\alpha}\varphi(-\beta)\mathrm{d}\beta + \int_{-H_s}^{H}\mu_{\mathrm{rev}}(\alpha)\mathrm{d}\alpha = \\ J(-H_s) + 2\int_{-H_s}^{H}\varphi(\alpha)[\Phi(H_s)-\Phi(-\alpha)]\mathrm{d}\alpha + \int_{-H_s}^{H}\mu_{\mathrm{rev}}(\alpha)\mathrm{d}\alpha \quad \text{(B.1)}$$

where $\pm H_s$ is the field at technical saturation and $\mu_{rev}(H)$ is the reversible permeability, assumed to depend on H only. We make the derivative of $J_{\uparrow}(H)$

$$\frac{\mathrm{d}J_{\uparrow}(H)}{\mathrm{d}H} = 2\,\frac{\mathrm{d}}{\mathrm{d}H}\int_{-H_s}^{H}\varphi(\alpha)\Phi(H_s)\mathrm{d}\alpha - 2\,\frac{\mathrm{d}}{\mathrm{d}H}\int_{-H_s}^{H}\varphi(\alpha)\Phi(-\alpha)\mathrm{d}\alpha + \\ +\mu_{\mathrm{rev}}(H) = 2\varphi(H)[\Phi(H_s)-\Phi(-H)] + \mu_{\mathrm{rev}}(H) \quad \text{(B.2)}$$

where we indicate with Φ the primitive of φ. To simplify, we pose the value of the primitive at saturation $\Phi(H_s) = 0$. We thus obtain

$$\frac{\mathrm{d}J_{\uparrow}(H)}{\mathrm{d}H} - \mu_{\mathrm{rev}}(H) = -2\varphi(H)\Phi(-H) \quad \text{(B.3)}$$

We write, in analogy with (B.1) the descending curve

$$J_{\downarrow}(H) = J(H_s) - \\ -2\int_{-H_s}^{-H}\varphi(-\beta)[\Phi(H_s)-\Phi(\beta)]\mathrm{d}(-\beta) - \int_{H}^{H_s}\mu_{\mathrm{rev}}(\alpha)\mathrm{d}\alpha\,. \quad \text{(B.4)}$$

We immediately obtain the difference $J_{\uparrow}(H) - J_{\downarrow}(H)$ by comparing ascending and descending major curves at the field H, through calculation of the areas correspondingly covered on the Preisach plane by the moving fronts of the switching hysterons. We have, in fact, that $J_{\uparrow}(H) - J_{\downarrow}(H)$ is obtained by integrating across the shaded area in Fig. B1

$$J_{\uparrow}(H) - J_{\downarrow}(H) = -2\int_{H}^{H_s}\varphi(\alpha)\mathrm{d}\alpha\int_{-H_s}^{H}\varphi(-\beta)\mathrm{d}\beta = \\ = 2[\Phi(H_s)-\Phi(H)][\Phi(-H)-\Phi(H_s)]. \quad \text{(B.5)}$$

By recalling the condition $\Phi(H_s) = 0$ and taking into account that, by virtue of the symmetry of the problem,

$$J_{\downarrow}(H) = -J_{\uparrow}(-H)\,, \quad \text{(B.6)}$$

we obtain

$$J_{\uparrow}(H) + J_{\uparrow}(-H) = -2\,\Phi(H)\cdot\Phi(-H) \quad , \quad \text{(B.7)}$$

which, in combination with (B.3), leads to the differential equation

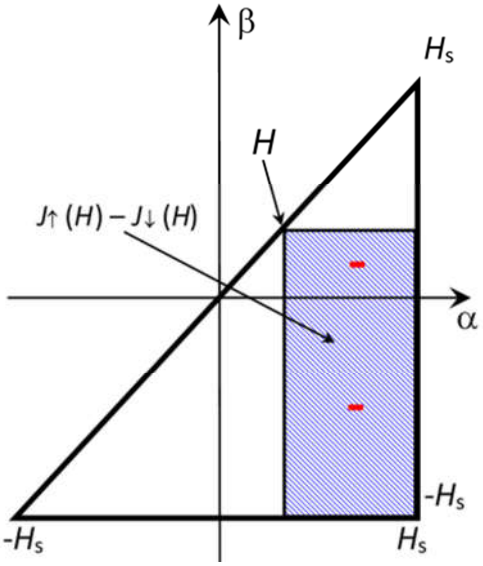

Fig. B.1. The difference $J_{\uparrow}(H) - J_{\downarrow}(H)$ between the polarization values attained along the ascending and descending branches of the limit hysteresis loop at the generic field H is obtained by integrating on the shaded area.

$$\frac{\mathrm{d}\Phi(H)/dH}{\Phi(H)} = \frac{\mathrm{d}J_{\uparrow}(H)/dH - \mu_{\mathrm{rev}}(H)}{J_{\uparrow}(H)+J_{\uparrow}(-H)} \quad , \quad \text{(B.8)}$$

where we have written $\varphi(H)$ as $\frac{\mathrm{d}\Phi(H)}{dH}$. We integrate (B.8) between the limits $H = 0$ and $H = H_{\mathrm{stat}}$

$$\ln\frac{\Phi(H)}{\Phi(0)} = \int_0^{H_{\mathrm{stat}}}\frac{\mathrm{d}J_{\uparrow}(H)/dH - \mu_{\mathrm{rev}}(H)}{J_{\uparrow}(H)+J_{\uparrow}(-H)}\,, \quad \text{(B.9)}$$

where, according to (B.7) and (B.6), $\Phi(0) = -\sqrt{J_{\downarrow}(H=0)}$, the negative value of $\Phi(0)$ descending from the previously assumed value $\Phi(H_s) = 0$. We consequently obtain

$$\Phi(H_{\mathrm{stat}}) = -\sqrt{J_{\downarrow}(H=0)}\,\exp\left[\int_0^{H_{stat}}\frac{\frac{dJ\uparrow}{dH} - \mu_{rev}(H)}{J_{\uparrow}(H)+J_{\uparrow}(-H)}\,dH\right] \quad \text{(B.10)}$$

and the Preisach distribution function as

$$\varphi(H_{\mathrm{stat}}) = \frac{\mathrm{d}\Phi(H_{\mathrm{stat}})}{dH_{\mathrm{stat}}}\,. \quad \text{(B.11)}$$